

SUPPLEMENTARY INFORMATION

Trifluoromethane Modification of Thermally Activated Delayed Fluorescence Molecules for High-efficiency Blue Organic Light-emitting Diodes

Masayuki Yokoyama,^{ab} Ko Inada,^{ac}, Youichi Tsuchiya,^{*ac} Hajime Nakanotani,^{*ac} and Chihaya Adachi,^{*acd}

^a Center for Organic Photonics and Electronics Research (OPERA), Kyushu University, 744 Motooka, Nishi-ku, Fukuoka 819-0395, Japan.

^b Functional Organic Materials Group, TOYOBO Co., Ltd., Research Center, 2-1-1 Katata, Otsu, Shiga 520-0292, Japan

^c JST, ERATO, Adachi Molecular Exciton Engineering Project, Kyushu University, 744 Motooka, Nishi-ku, Fukuoka 819-0395, Japan.

^d International Institute for Carbon Neutral Energy Research (WPI-I2CNER), Kyushu University, 744 Motooka, Nishi-ku, Fukuoka 819-0395, Japan.

E-mails:

tsuchiya@opera.kyushu-u.ac.jp,
nakanotani@cstf.kyushu-u.ac.jp,
adachi@cstf.kyushu-u.ac.jp

1. Experimental details

The absorption spectra were measured using a UV-visible spectrophotometer UV-2550 (Shimadzu) at room temperature. The emission spectra were measured using a FluoroMax-4 (Horiba Jobin Yvon) at room temperature. Thin-film samples (**4CzIPN**, **1**, **2**, **4CzTPN**, **3**, **4** pristine films and 10 wt% PPT doped films, 50 nm thicknesses) were deposited by vacuum evaporation under high vacuum ($< 5 \times 10^{-4}$ Pa) onto the substrates. The photoluminescence quantum yield (PLQY, ϕ_{PL}) was measured using measurement system C11347-11 (Hamamatsu Photonics) under argon flow. The transient photoluminescence decay characteristics of film samples were recorded using a Quantaurus-Tau fluorescence lifetime measurement system C11367-03 (Hamamatsu Photonics). The prompt and delayed PL spectra and phosphorescent spectra of the doped films were measured under vacuum using a streak camera system C4334 (Hamamatsu Photonics) with an excitation wavelength of 337 nm. Ionic potential of the materials was measured using photoemission yield spectrometer AC-3 (Riken Keiki). The photo-degradation was measured by light irradiation using MAX-303 (Asahi Spectra) with 300-400 band pass filter and light intensity control feedback unit. The initial irradiation light intensity was measured by C9536_H9958 (Hamamatsu Photonics) and the emission was continuously recorded by PMA-12 (Hamamatsu Photonics). OLED samples were fabricated by thermal evaporation onto clean indium tin oxide-coated glass substrates. The current density-voltage-luminance (J-V-L) and CIE characteristics were measured using an external quantum efficiency measurement system (C9920-12, Hamamatsu Photonics). Quantum chemical calculations were performed using the Gaussian 16 Rev. A.03. Geometry optimization of the ground state was carried out using the B3LYP functional with the 6-31+G(d) basis set, and S_1 and T_1 states were calculated with time-dependent DFT method using the same functional with the 6-31G(d) basis set.

2. Synthesis and characterization

Sodium hydride (60 wt%, dispersion in mineral oil, sigma-aldrich), tetrafluoroisophthalonitrile, tetrafluoroterephthalonitrile (tokyo chemical industry co., ltd.), THF (super dehydrated, fujifilm wako pure chemical corporation), **TBPe** and **Flrpic** (luminescence technology corp., Fig. S1) were used as received. All reactions were carried out under N₂ atmosphere. In general, evaporation and concentration of solvents were carried out under reduced pressure below 50 °C, unless otherwise noted. ¹H and ¹⁹F NMR spectra were determined using a Bruker Biospin Avance III 500 spectrometer or an Agilent VNMRS 400 spectrometer with chloroform-d, DMSO-d₆ or acetone-d₆ as a solvent. Coupling constants (*J*) are given in hertz (Hz) and are quoted to the nearest 0.5 Hz. Peak multiplicities are described in the following way: s, singlet; d, doublet; dd, doubledoublet; t, triplet; m, multiplet. Mass spectra were measured in positive-ion atmospheric pressure solid analysis probe (ASAP) mode on a Waters 3100 mass detector. Elemental analysis was performed by the Service Center of the Elementary Analysis of Organic Compounds affiliated with the Faculty of Sciences at Kyushu University.

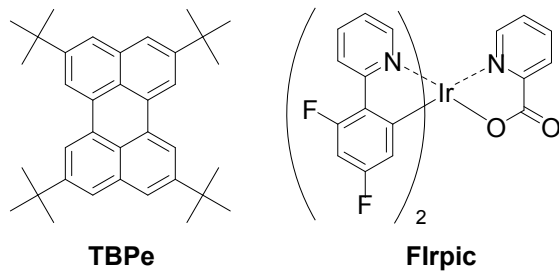
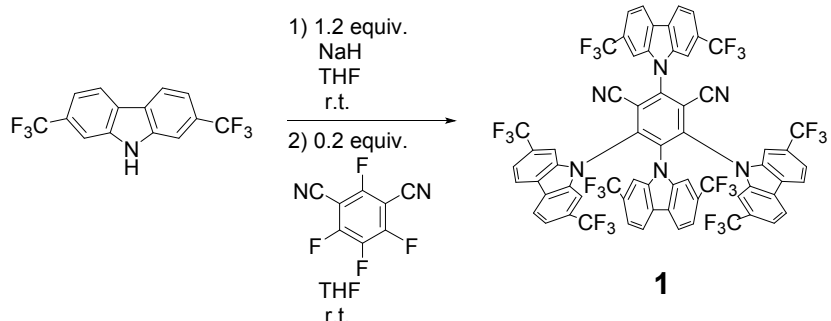


Fig. S1. Chemical structures of **TBPe** and **Flrpic**.

2.1 1,2,3,5-tetrakis(2,7-bis(trifluoromethyl)carbazol-9-yl)-4,6-dicyanobenzene (1)



To a solution of 2,7-bis(trifluoromethyl)carbazole (3.03 g, 10.0 mmol) in THF (100 ml) was portionwisely added sodium hydride (480 mg, 60wt% dispersion in mineral oil, 12.0 mmol), then the mixture was stirred for 1 h. After stirring, tetrafluoroisophthalonitrile (400 mg, 2.00 mmol) was added to the solution dropwisely, and then resulted mixture was stirred at room temperature for 18 h. The reaction was quenched by adding water. The precipitate was filtered and washed with water and chloroform to give light yellow powder (2.60 g, 97.5 % yield). The product was further purified by sublimation before measurements.

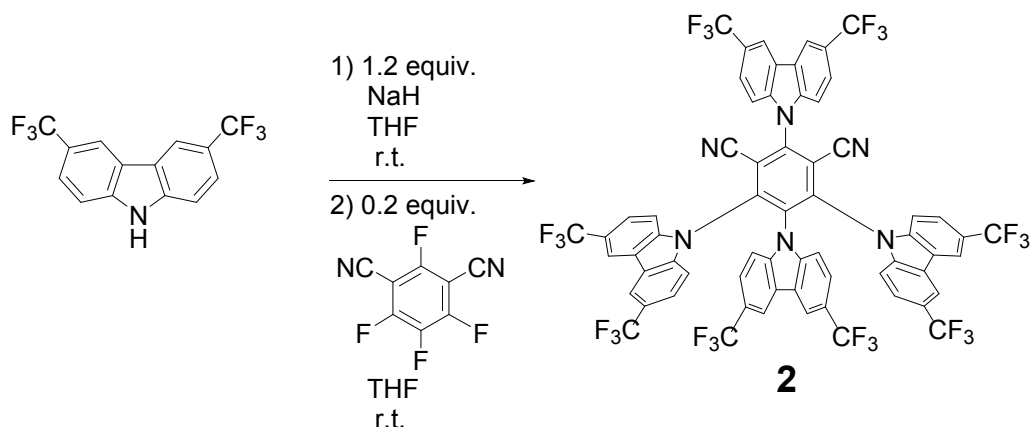
¹H NMR (500 MHz, acetone-d₆): δ = 7.33 (dd, *J* = 8.5, 1.0 Hz, 2H), 7.62 (dd, *J* = 8.5, 1.0 Hz, 4H), 7.89 (s, 2H), 7.90 (s, 4H), 7.93 (d, *J* = 8.5 Hz, 2H), 7.98 (dd, *J* = 8.5, 1.0 Hz, 2H), 8.05 (s, 2H), 8.33 (d, *J* = 8.5 Hz, 4H), 8.80 (d, *J* = 8.5 Hz, 2H).

¹⁹F NMR (400 MHz, acetone-d₆): δ = -61.73, -62.14, -62.21.

MS (ASAP): *m/z* 1333 [M⁺].

Anal. Calcd. for C₆₄H₂₄F₂₄N₆ (%): C 57.67, H 1.81, N 6.31; Found C 57.63, H 1.89, N 6.33.

2.2 1,2,3,5-tetrakis(3,6-bis(trifluoromethyl)carbazol-9-yl)-4,6-dicyanobenzene (2)



To a solution of 3,6-bis(trifluoromethyl)carbazole (2.12 g, 6.99 mmol) in THF (70 ml) was portionwisely added sodium hydride (336 mg, 60wt% dispersion in mineral oil, 8.40 mmol), then the mixture was stirred for 1 h. After stirring, tetrafluoroisophthalonitrile (280mg, 1.40 mmol) was added to the solution dropwisely, and then resulted mixture was stirred at room temperature for 13 h. The reaction was quenched by adding water. The precipitate was filtered and washed with water and isopropanol to give light yellow powder (1.86 g, 100 % yield). The product was further purified by sublimation before measurements.

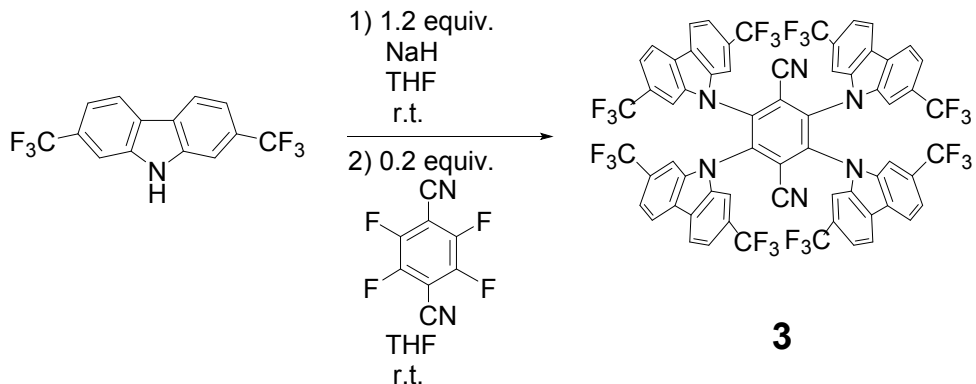
¹H NMR (500 MHz, DMSO-d₆): δ = 7.16 (dd, *J* = 8.5, 1.5 Hz, 2H), 7.60–7.68 (m, 6H), 7.98 (d, *J* = 8.5 Hz, 4H), 8.20 (s, 2H), 8.30 (dd, *J* = 8.5, 1.5 Hz, 2H), 8.40 (d, *J* = 8.5 Hz, 2H), 8.63 (s, 4H), 9.19 (s, 2H).

¹⁹F NMR (400 MHz, DMSO-d₆): δ = -59.12, -59.46, -59.68.

MS (ASAP): m/z 1333 [M $^+$].

Anal. Calcd. for $C_{64}H_{24}F_{24}N_6$ (%): C 57.67, H 1.81, N 6.31; Found: C 57.91, H 1.81, N 6.30.

2.3 1,2,4,5-tetrakis(2,7-bis(trifluoromethyl)carbazol-9-yl)-3,6-dicyanobenzene (3)



To a solution of 2,7-bis(trifluoromethyl)carbazole (3.03 g, 10.0 mmol) in THF (100 ml) was portionwisely added sodium hydride (480 mg, 60wt% dispersion in mineral oil, 12.0 mmol), then the mixture was stirred for 1 h. After stirring, tetrafluoroterephthalonitrile (400 mg, 2.00 mmol) was added to the solution dropwisely, and then resulted mixture was stirred at room temperature for 18 h. The reaction was quenched by adding water. The precipitate was filtered and washed with water and chloroform to give yellow powder (2.57 g, 96.4 % yield). The product was further purified by sublimation before measurements.

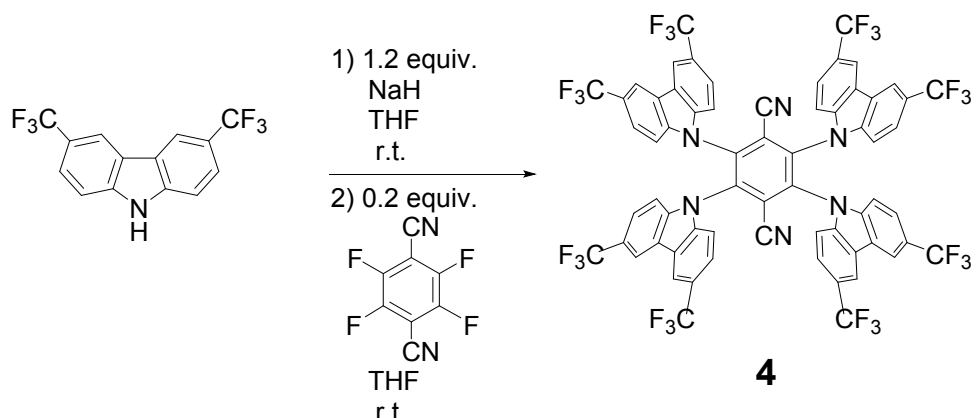
¹H NMR (500 MHz, acetone-d₆): δ = 7.66 (dd, *J* = 8.0, 1.5 Hz, 8H), 8.04 (d, *J* = 1.5Hz, 8H), 8.35 (d, *J* = 8.0 Hz, 8H).

¹⁹F NMR (400 MHz, acetone-d₆): δ = -61.91.

MS (ASAP): *m/z* 1333 [M⁺].

Anal. Calcd. for C₆₄H₂₄F₂₄N₆ (%): C 57.67, H 1.81, N 6.31; Found C 57.73, H 1.76, N 6.48.

2.3 1,2,4,5-tetrakis(3,6-bis(trifluoromethyl)carbazol-9-yl)-3,6-dicyanobenzene (4)



To a solution of 3,6-bis(trifluoromethyl)carbazole (2.12 g, 6.99 mmol) in THF (70 ml) was portionwisely added sodium hydride (336 mg, 60wt% dispersion in mineral oil, 8.40 mmol), then the mixture was stirred for 1 h. After stirring, tetrafluoroterephthalonitrile (280 mg, 1.40 mmol) was added to the solution dropwisely, and then resulted mixture was stirred at room temperature for 18 h. The reaction was quenched by adding water. The precipitate was filtered and washed with water and chloroform to give yellow powder (1.85 g, 99.1 % yield). The product was further purified by sublimation before measurements.

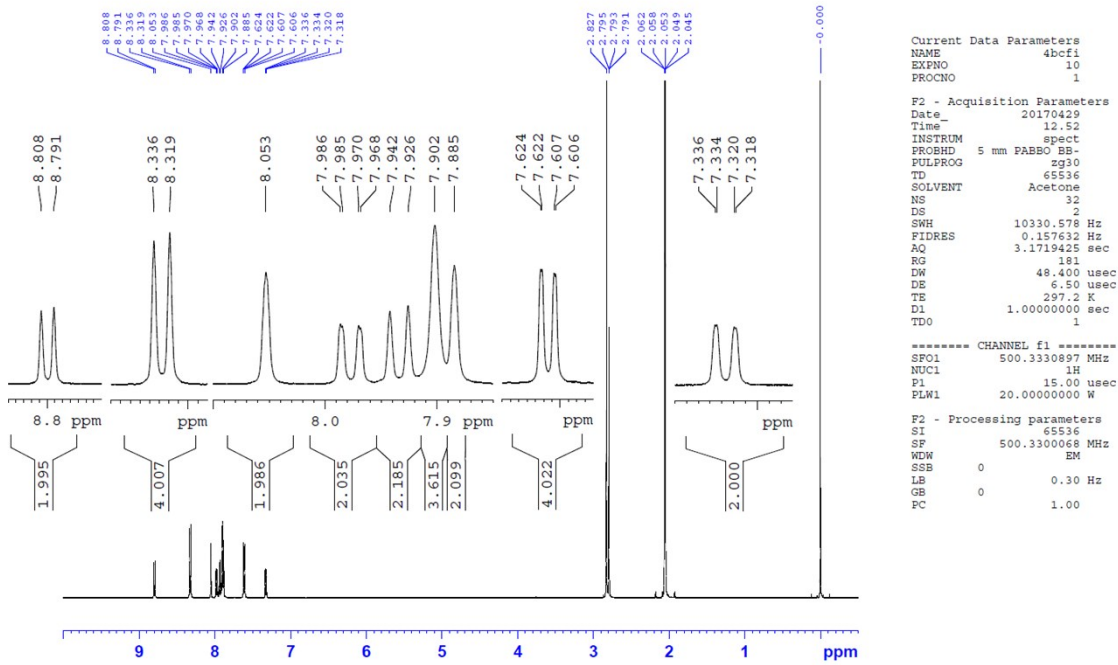
¹H NMR (500 MHz, acetone-d₆): δ = 7.61 (dd, J = 8.5, 2.5 Hz, 8H), 7.91 (d, J = 8.5 Hz, 8H), 8.51 (d, J = 2.5 Hz, 8H).

¹⁹F NMR (400 MHz, acetone-d₆): δ = -61.55.

MS (ASAP): *m/z* 1333 [M⁺].

Anal. Calcd. for C₆₄H₂₄F₂₄N₆ (%): C 57.67, H 1.81, N 6.31; Found C 57.81, H 1.83, N 6.26.

¹H NMR



¹⁹F NMR

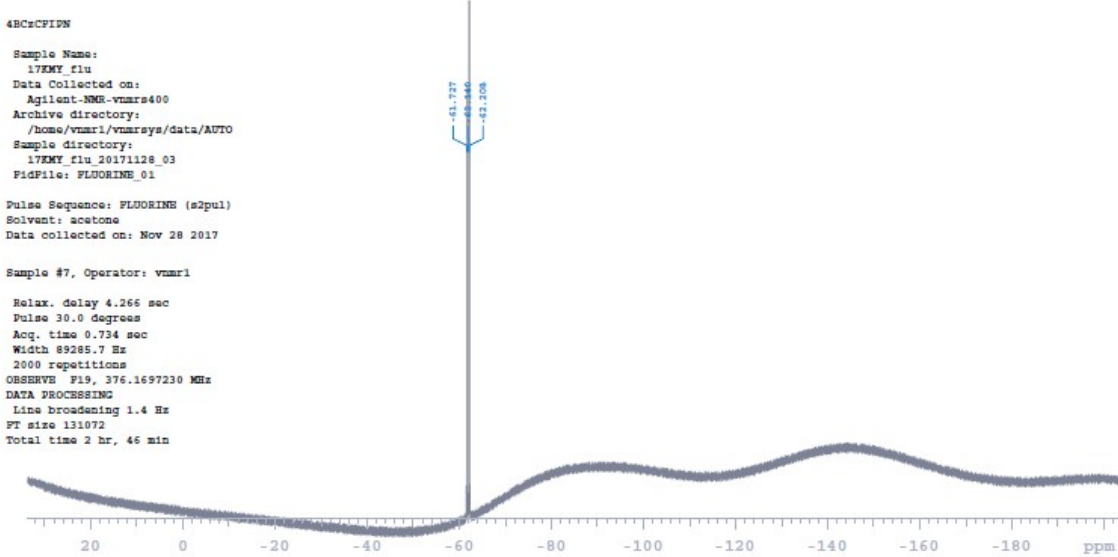
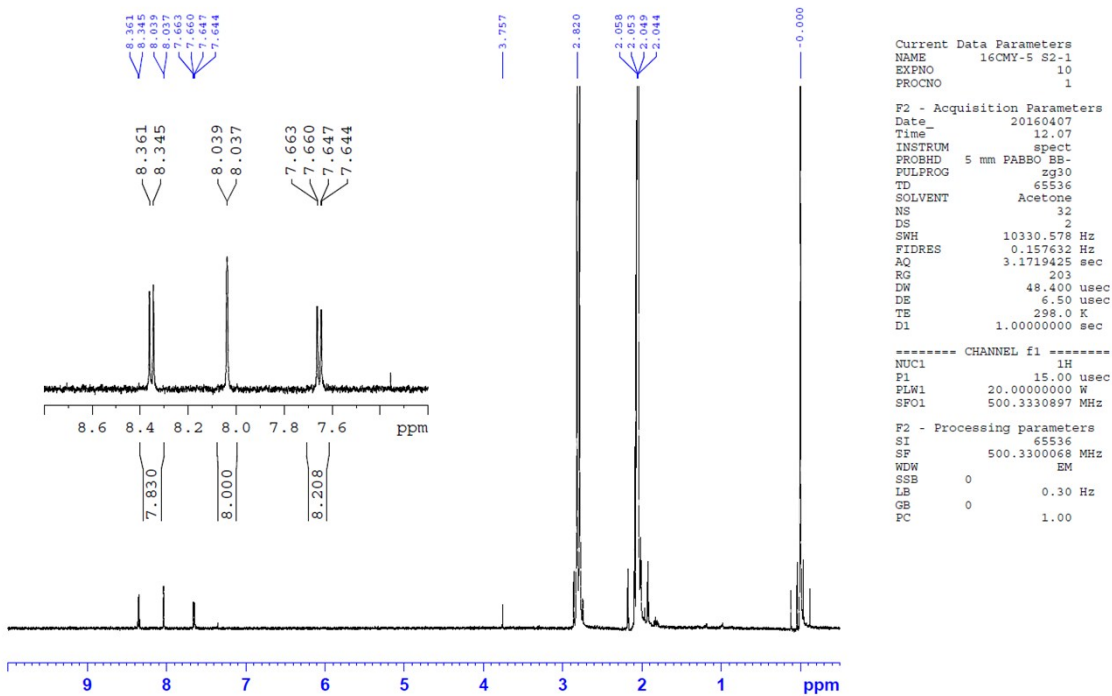


Fig. S2. ¹H and ¹⁹F NMR spectra of **1**

¹H NMR



¹⁹F NMR

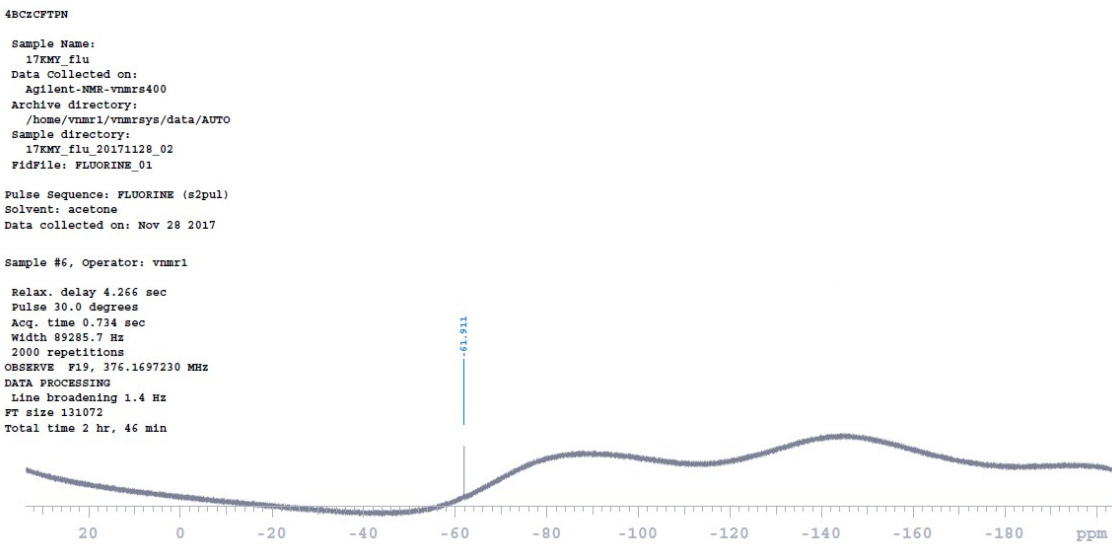
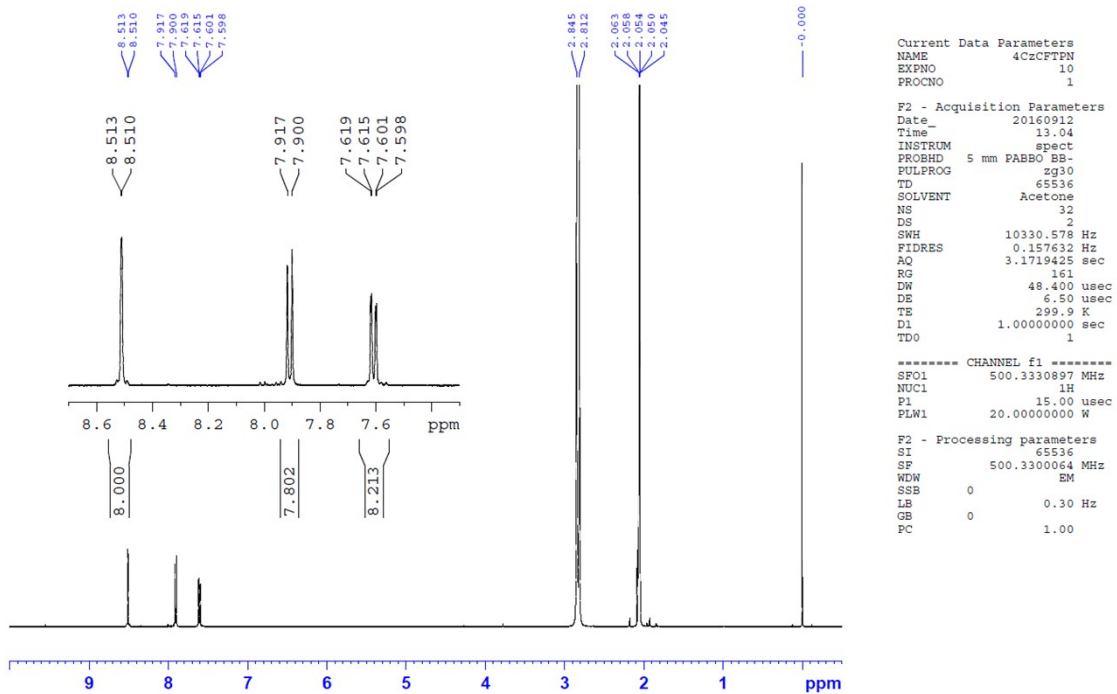


Fig. S4. ¹H and ¹⁹F NMR spectra of **3**

¹H NMR



¹⁹F NMR

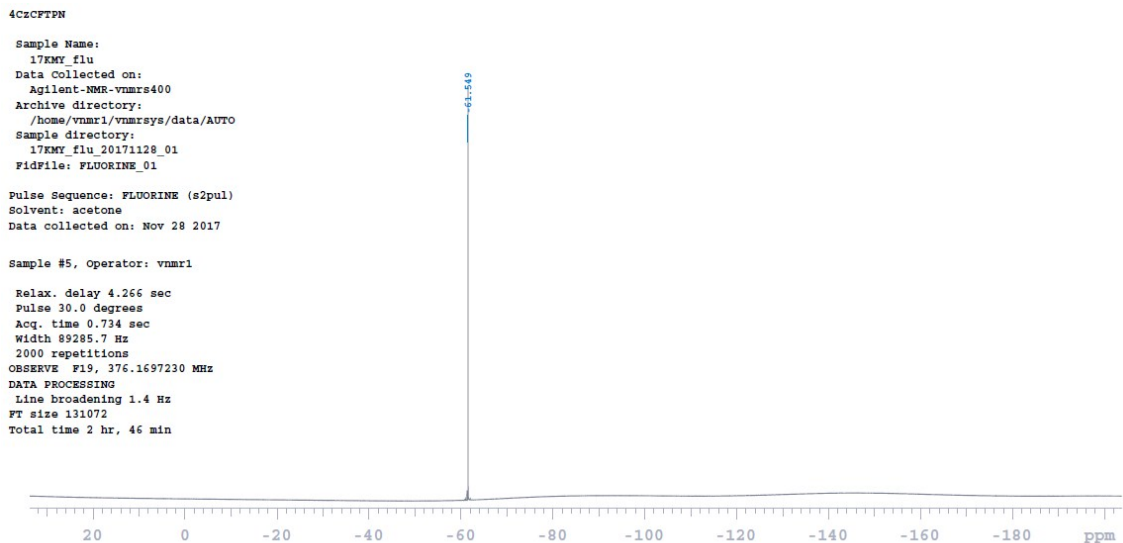


Fig. S5. ¹H and ¹⁹F NMR spectra of **4**

Table S1. DFT calculations of **4CzIPN**, **1**, **2**, **4CzTPN**, **3** and **4** (B3LYP/6-31+G(d)// B3LYP/6-31G(d)) using Gaussian 16, Rev. A.03.

Emitter	HOMO (eV)	LUMO (eV)	E_g (eV)	S_1 (eV)	T_1 (eV)	ΔE_{ST} (eV)	f	Θ_1 (°)	Θ_2 (°)	Θ_3 (°)	Θ_4 (°)
4CzIPN	-5.67	-2.56	3.11	2.44	2.32	0.12	0.094	70	65	63	63
1	-6.43	-3.32	3.11	2.45	2.37	0.09	0.074	66	70	68	70
2	-6.78	-3.57	3.20	2.60	2.49	0.11	0.091	71	65	64	64
4CzTPN	-5.73	-2.82	2.91	2.25	2.15	0.10	0.101	67	67	67	67
3	-6.42	-3.50	2.92	2.27	2.17	0.10	0.099	67	70	71	69
4	-6.83	-3.81	3.02	2.43	2.33	0.10	0.099	67	67	67	67

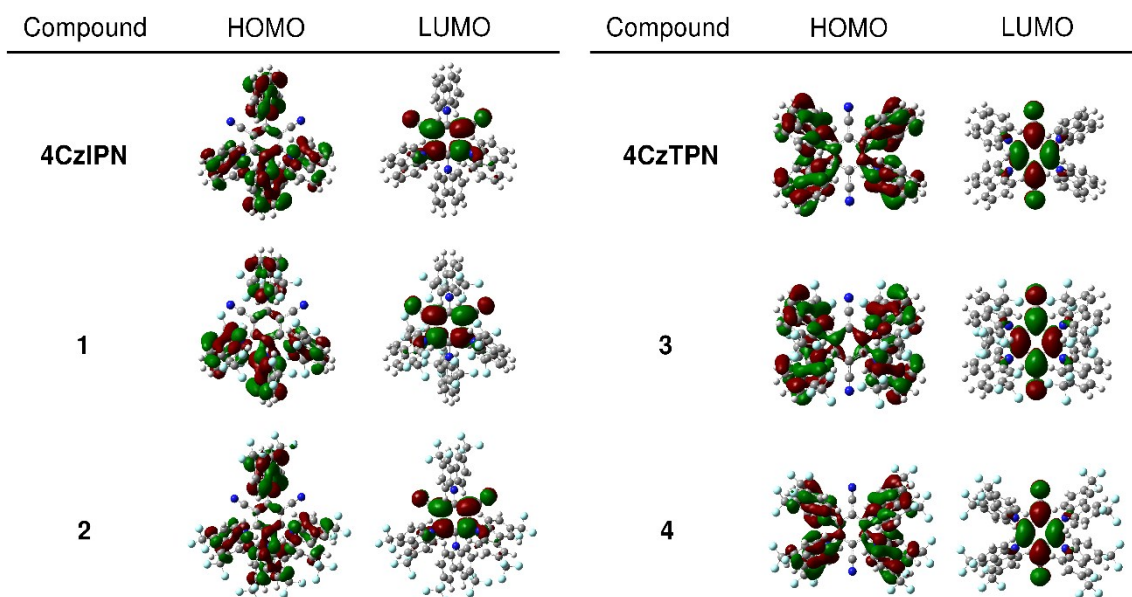
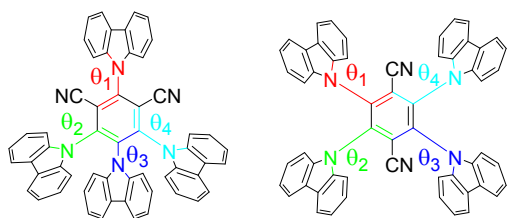


Fig. S6. HOMO and LUMO distributions for **1-4**, **4CzIPN** and **4CzTPN** (B3LYP/6-31G(d)) using Gaussian 16, Rev. A.03.

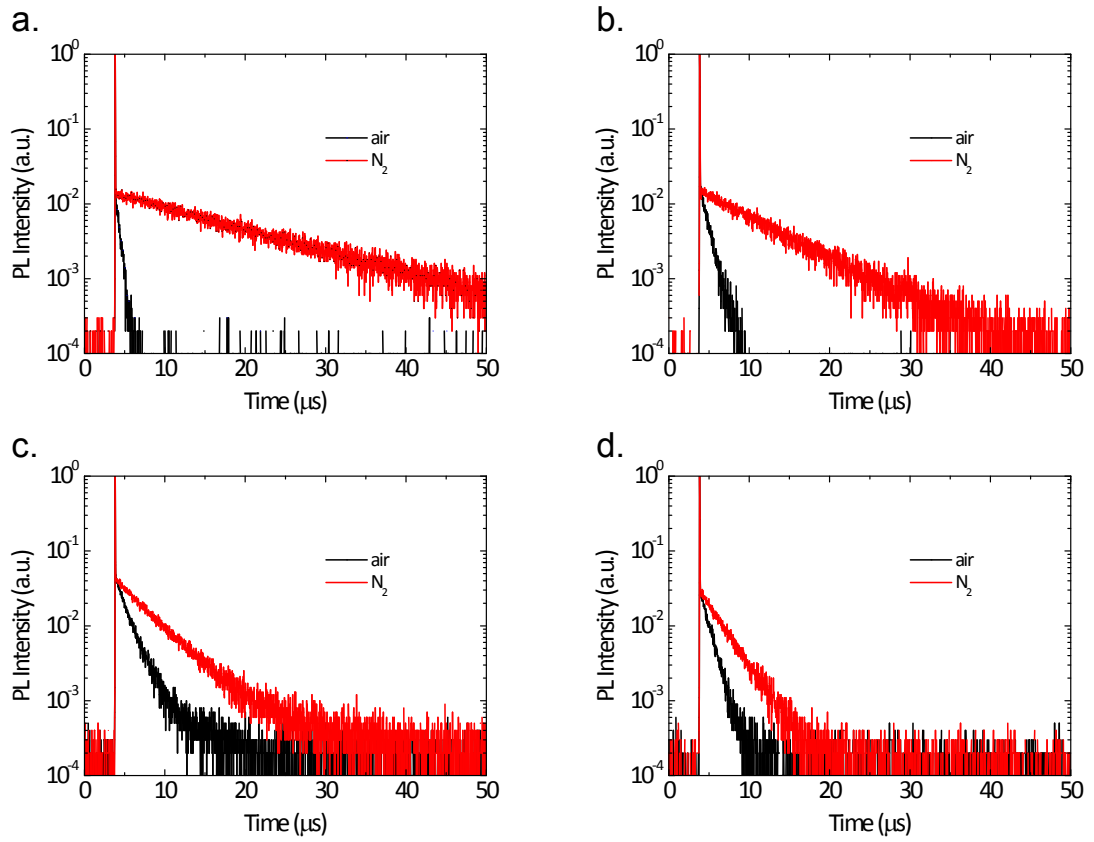
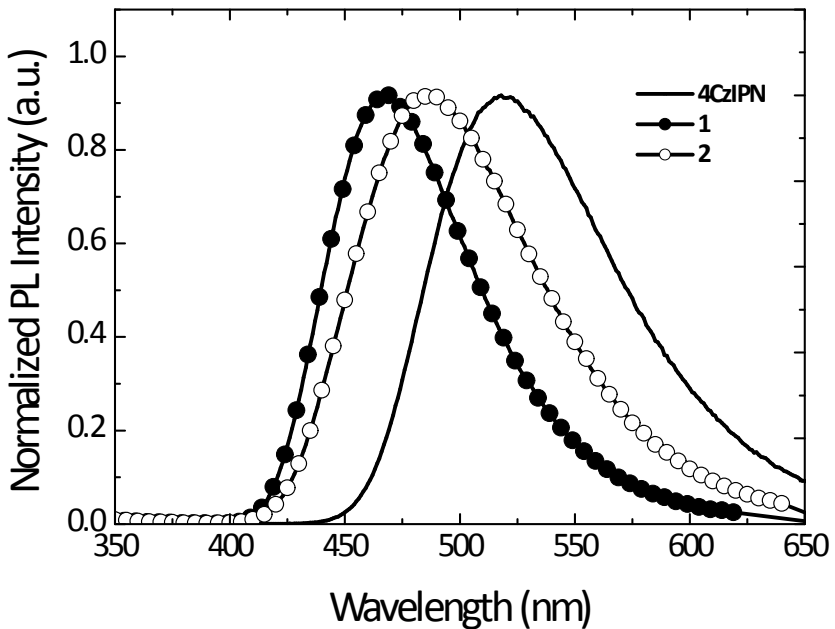


Fig. S7. Transient PL decay curve of **1** (a), **2** (b), **3** (c) and **4** (d) in toluene (1.0×10^{-5} M); black line; air saturated, red line; N_2 saturated.

a.



b.

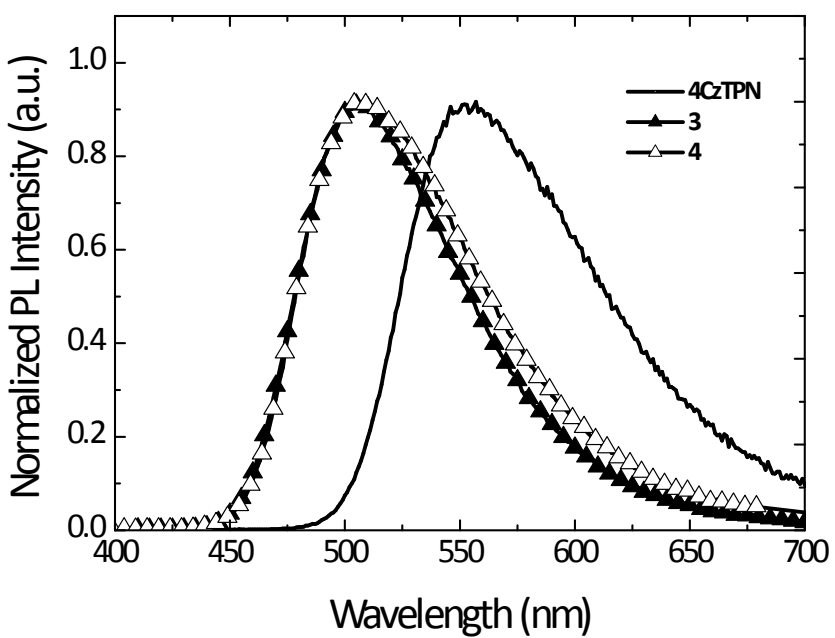


Fig. S8. PL spectra of 10 wt% doped PPT films; (a) 4CzIPN, **1** and **2**; (b) 4CzTPN, **3** and **4**.

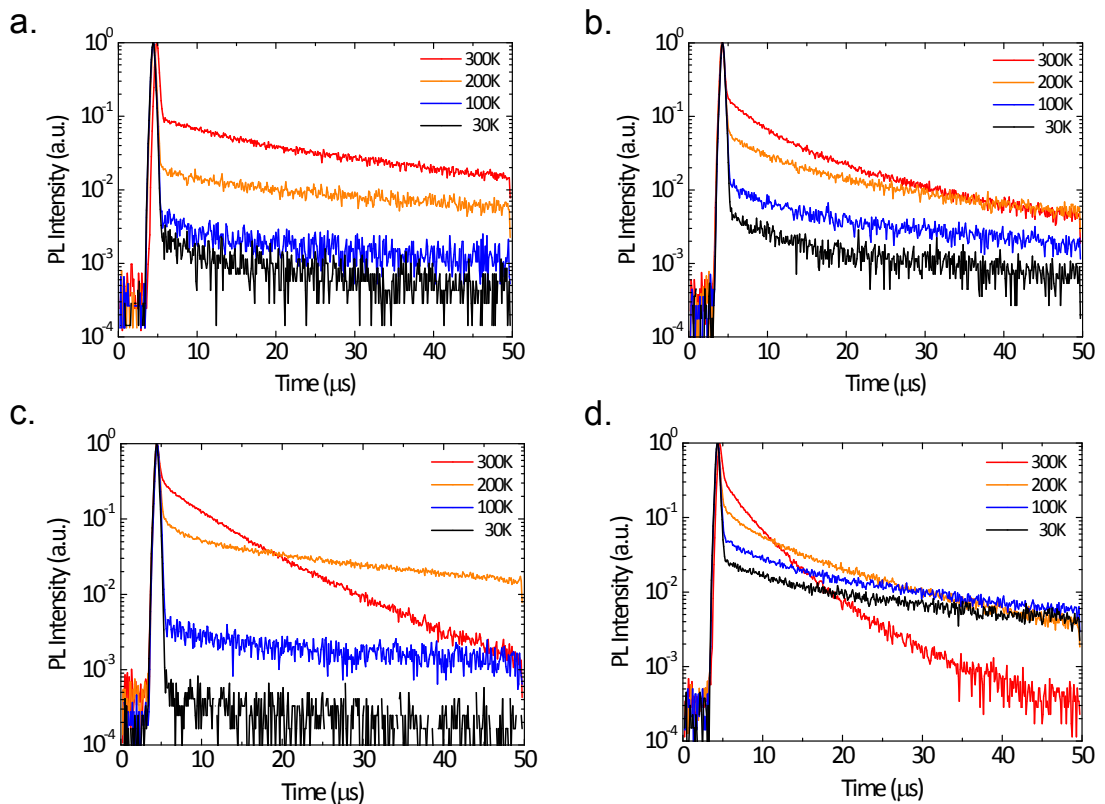


Fig. S9. Transient PL decay curves of 10 wt% doped PPT films for **1** (a), **2** (b), **3** (c) and **4** (d) at 30, 100, 200, 300 K.

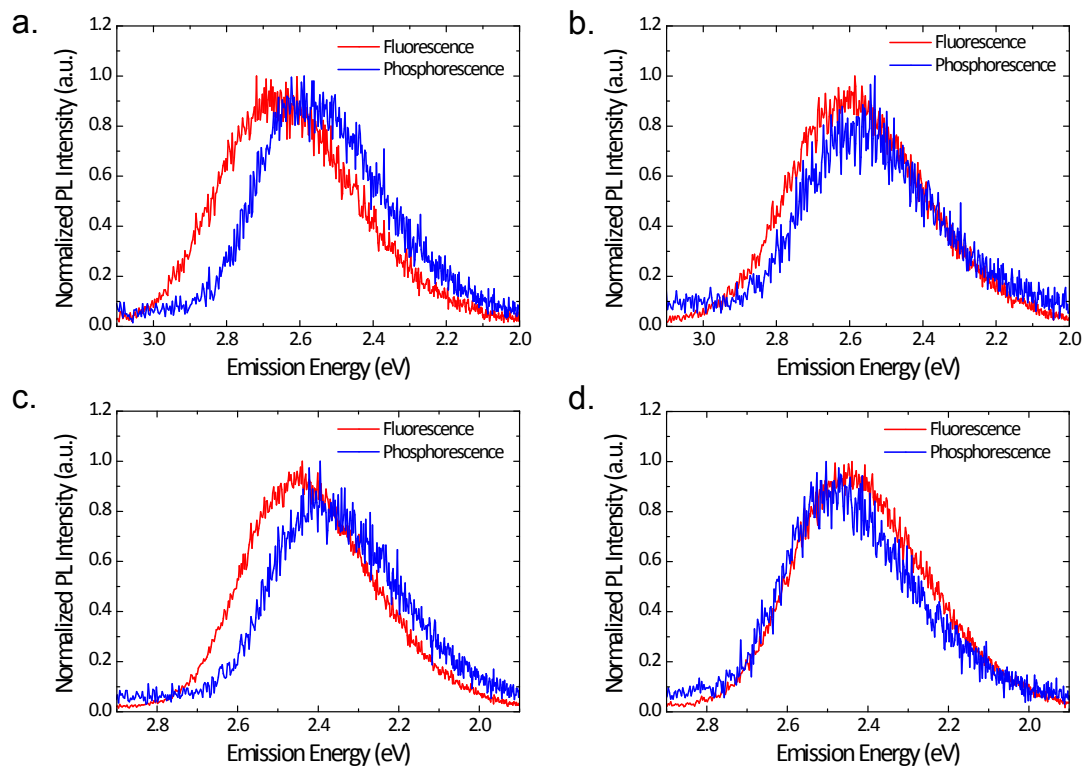


Fig. S10. Prompt fluorescent spectra (<10 ns) at 300 K and phosphorescence spectra (1-10 ms) of 10 wt% doped PPT films for **1** (a), **2** (b), **3** (c) and **4** (d) at 30 K.

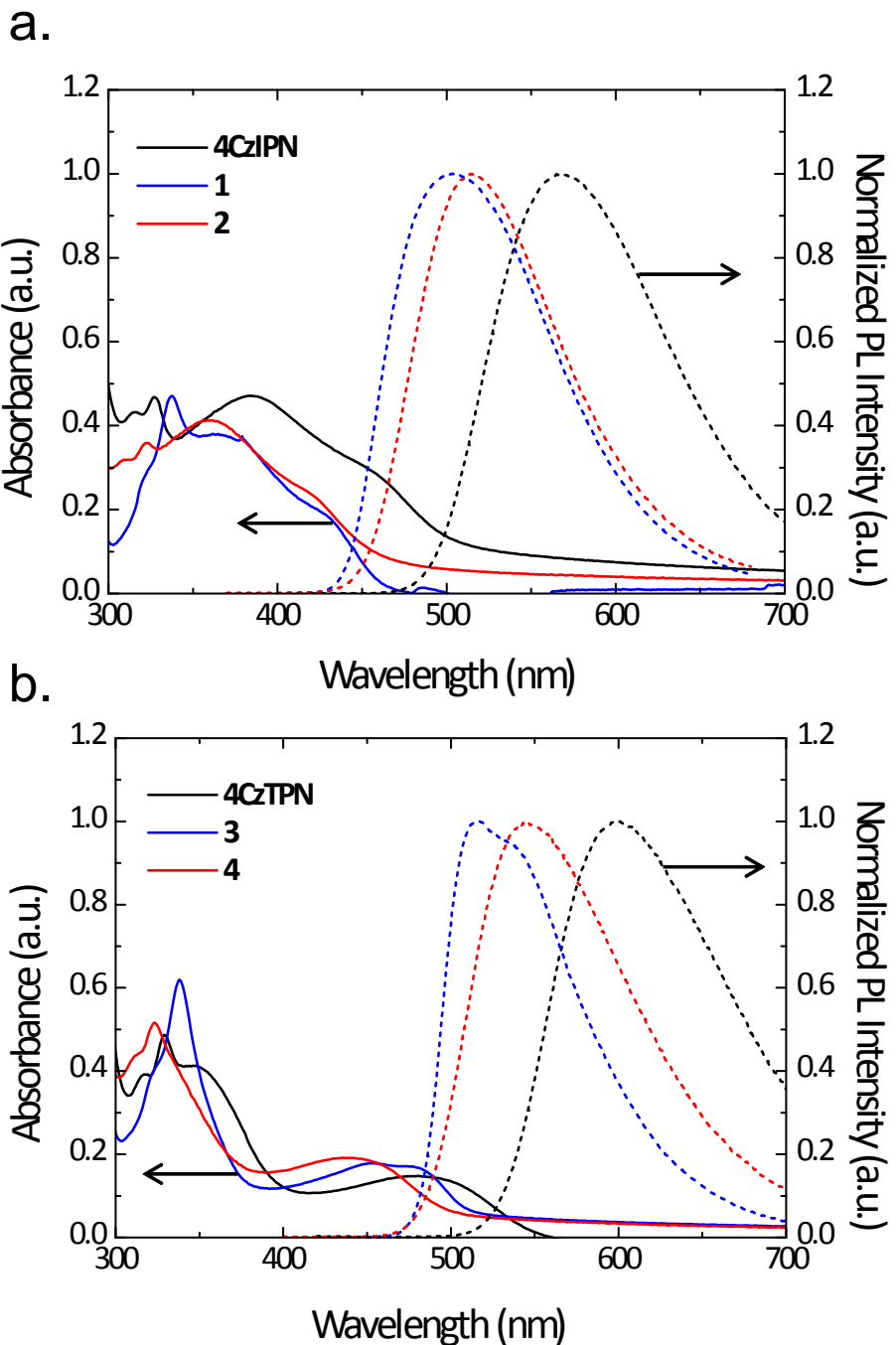


Fig. S11. UV-vis absorption (solid line) and PL spectra (broken line) of pristine films; (a) **4CzIPN**, **1** and **2**; (b) **4CzTPN**, **3** and **4**.

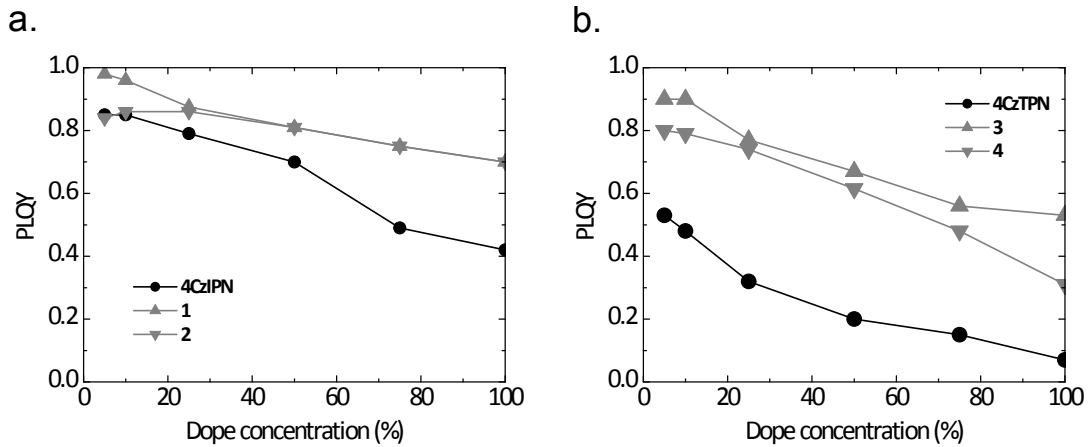


Fig. S12. PLQY of emitter doped PPT films with various doping concentration (5, 10, 25, 50, 75 wt%) and pristine film (100 wt%); (a) 4CzIPN, 1 and 2; (b) 4CzTPN, 3 and 4.

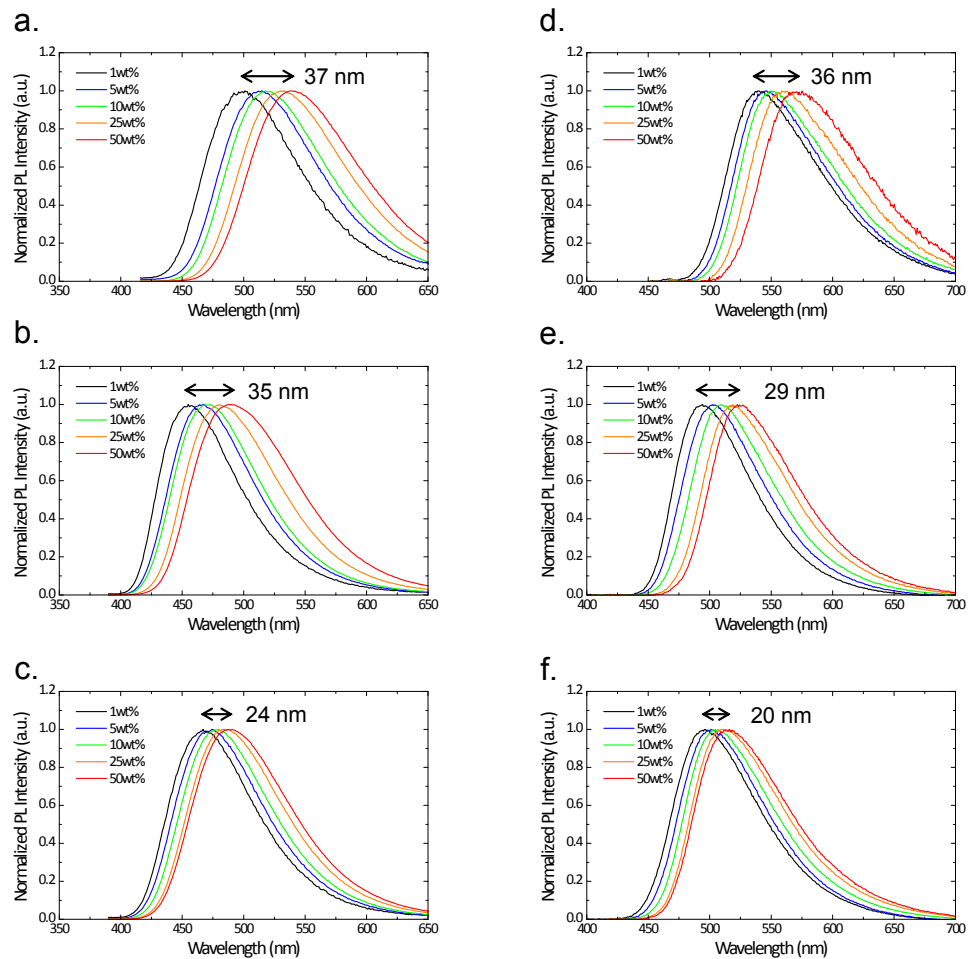


Fig. S13. PL spectra of emitter doped PPT films with various doping concentration; (a) 4CzIPN; (b) 1; (c) 2; (d) 4CzTPN; (e) 3; (f) 4.

Table S2. PL peak wavelength of pristine films and 10 wt% doped PPT films of **1-4**, **4CzIPN** and **4CzTPN**.

Emitter	pristine	10 wt%	difference
	film	doped film	
	λ_{PL}	λ_{PL}	$\Delta\lambda_{PL}$
(nm)	(nm)	(nm)	
4CzIPN	567	524	43
1	503	469	34
2	515	482	33
4CzTPN	601	557	44
3	516	504	12
4	546	507	39

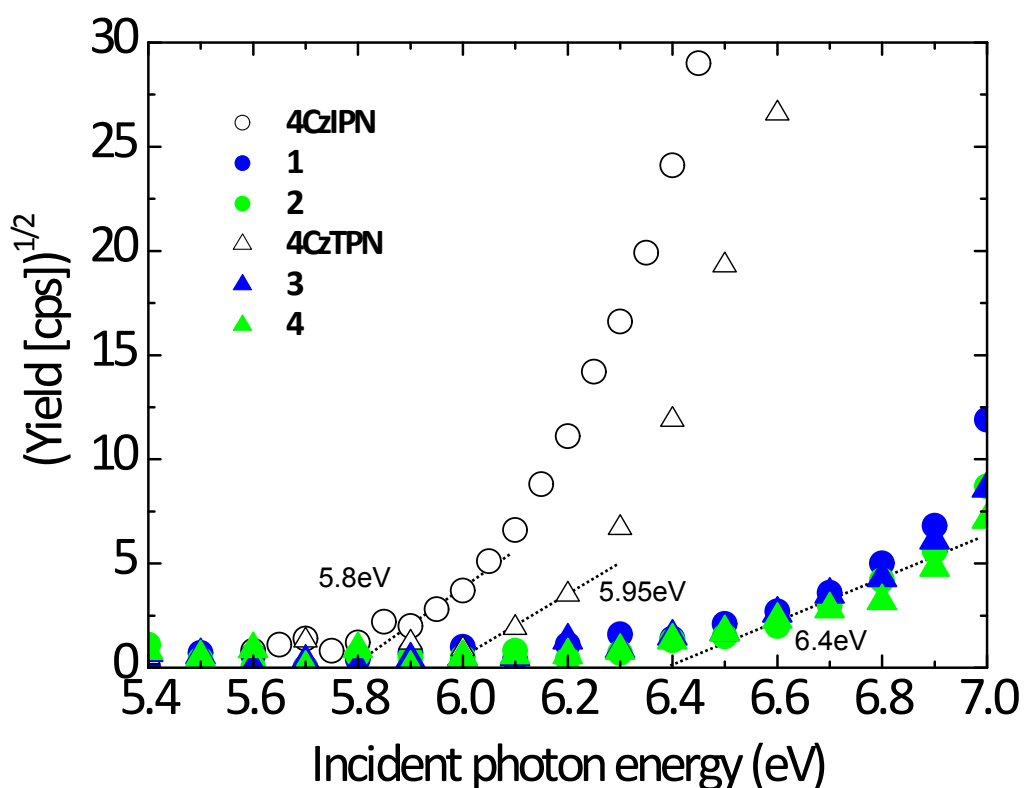


Fig. S14. Photoelectron yield spectroscopy in air of **1-4**, **4CzIPN** and **4CzTPN** pristine films (UV light source intensity, 10 nW).

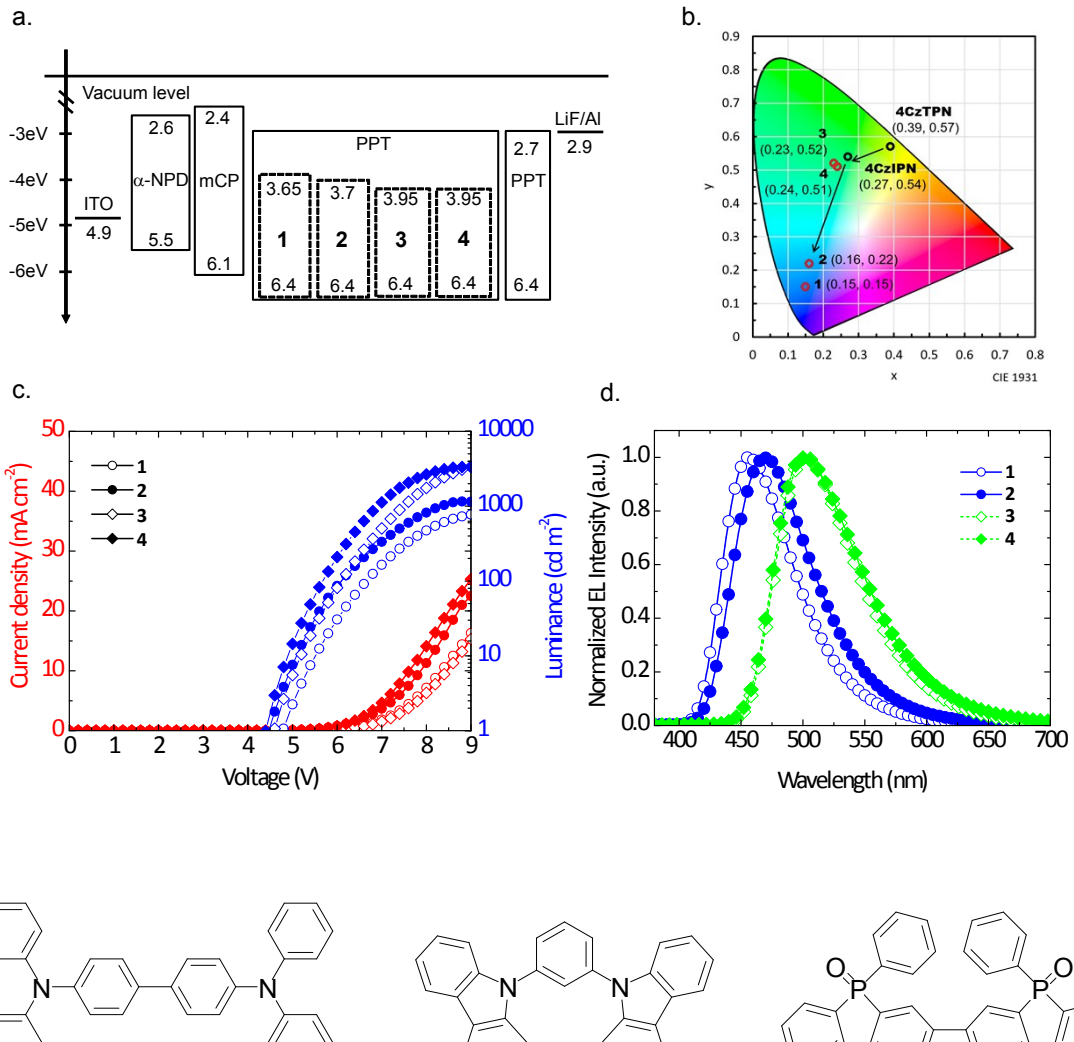


Fig. S15. Electroluminescence characteristics of OLED using **1-4** as an emitter; (a) Energy diagram; (b) CIE diagram (CIE1931); (c) Current density-voltage-luminance characteristics; (d) EL spectra.

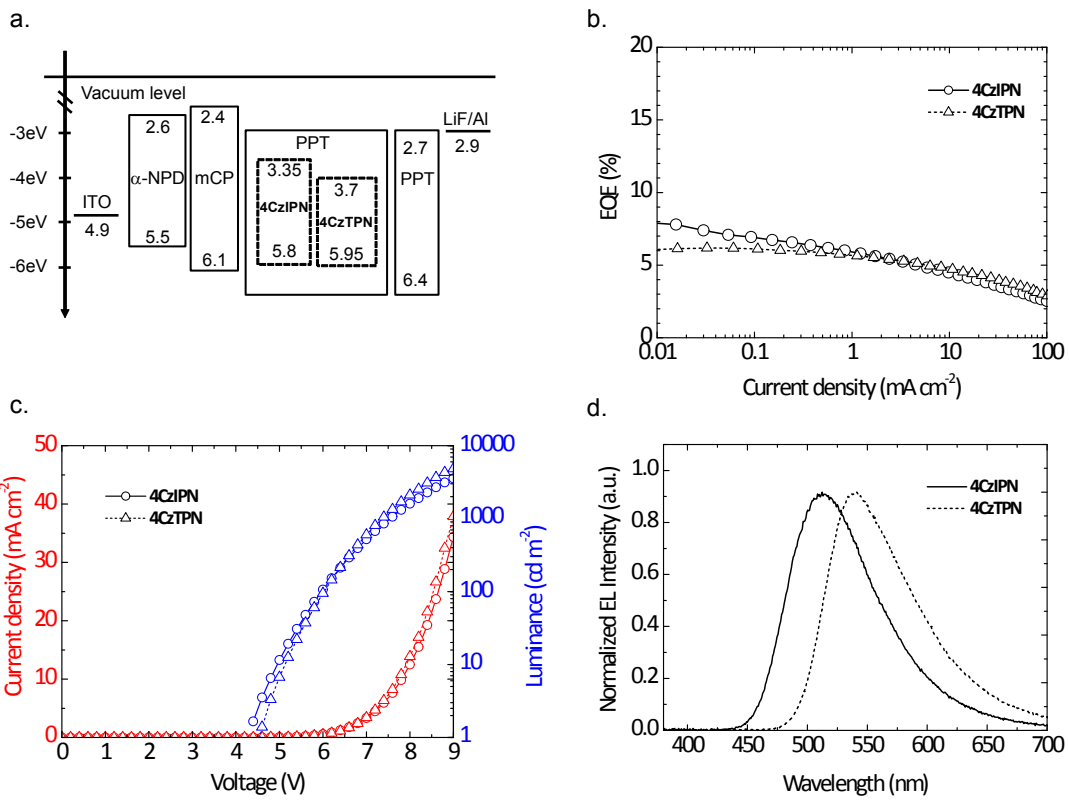
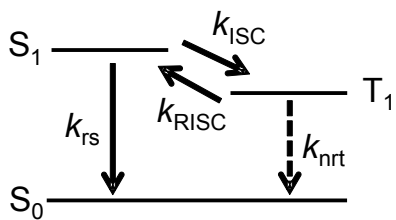


Fig. S16. Electroluminescence characteristics of OLED using **4CzIPN**, **4CzTPN** as an emitter; (a) Energy diagram; (b) EQE-current density characteristics; (c) Current density-voltage-luminance characteristics; (d) EL spectra.

Table S3. Kinetic parameters of 10 wt% doped PPT films for **1-4**, **4CzIPN** and **4CzTPN**.

Emitter	k_{rs}	k_{ISC}	k_{RISC}	k_{nrt}
4CzIPN	5.62×10^6	7.44×10^7	3.58×10^6	4.77×10^4
1	4.00×10^6	2.05×10^8	4.21×10^6	3.96×10^3
2	3.66×10^6	1.04×10^8	4.19×10^6	2.38×10^4
4CzTPN	3.02×10^6	1.42×10^8	9.15×10^6	2.15×10^5
3	3.43×10^6	2.78×10^8	1.00×10^7	3.01×10^4
4	6.72×10^6	1.16×10^8	4.57×10^6	7.46×10^5



The respective rate constants of the prompt and delayed fluorescence components (k_p and k_d), in the presence of mutual ISC between the singlet and triplet states, are given by¹

$$k_p = \frac{1}{\tau_p} = k_{rs} + k_{ISC} \quad (1)$$

$$k_d = \frac{1}{\tau_d} = k_{nrt} + \left(1 - \frac{k_{ISC}}{k_{rs} + k_{ISC}}\right)k_{RISC} \quad (2)$$

The PL quantum efficiencies of the prompt and delayed components (ϕ_p and ϕ_d) are given by

$$\phi_p = \frac{k_{rs}}{k_{rs} + k_{ISC}} \quad (3)$$

$$\phi_d = \sum_{k=1}^{\infty} (\phi_{ISC}\phi_{RISC})^k \phi_p \quad (4)$$

where ϕ_{ISC} and ϕ_{RISC} are the quantum efficiencies for ISC and RISC, respectively. The following equation is obtained from equations (1)-(4):

$$k_{RISC} = \frac{k_p k_d \phi_d}{k_{ISC} \phi_p} \quad (5)$$

Thus, k_{RISC} can be estimated from the experimentally observable rate constants and the PL quantum efficiencies of the prompt and delayed components.

References

- 1 H. Uoyama, K. Goushi, K. Shizu, H. Nomura and C. Adachi, *Nature*, 2012, **492**, 234–238.

Full Gaussian references

Gaussian 16, Revision A.03, M. J. Frisch, G. W. Trucks, H. B. Schlegel, G. E. Scuseria, M. A. Robb, J. R. Cheeseman, G. Scalmani, V. Barone, G. A. Petersson, H. Nakatsuji, X. Li, M. Caricato, A. V. Marenich, J. Bloino, B. G. Janesko, R. Gomperts, B. Mennucci, H. P. Hratchian, J. V. Ortiz, A. F. Izmaylov, J. L. Sonnenberg, D. Williams-Young, F. Ding, F. Lipparini, F. Egidi, J. Goings, B. Peng, A. Petrone, T. Henderson, D. Ranasinghe, V. G. Zakrzewski, J. Gao, N. Rega, G. Zheng, W. Liang, M. Hada, M. Ehara, K. Toyota, R. Fukuda, J. Hasegawa, M. Ishida, T. Nakajima, Y. Honda, O. Kitao, H. Nakai, T. Vreven, K. Throssell, J. A. Montgomery, Jr., J. E. Peralta, F. Ogliaro, M. J. Bearpark, J. J. Heyd, E. N. Brothers, K. N. Kudin, V. N. Staroverov, T. A. Keith, R. Kobayashi, J. Normand, K. Raghavachari, A. P. Rendell, J. C. Burant, S. S. Iyengar, J. Tomasi, M. Cossi, J. M. Millam, M. Klene, C. Adamo, R. Cammi, J. W. Ochterski, R. L. Martin, K. Morokuma, O. Farkas, J. B. Foresman, and D. J. Fox, Gaussian, Inc., Wallingford CT, 2016.